New Journal of Physics
The open access journal at the forefront of physics

Deutsche Physikalische Gesellschaft DPG IOP Institute of Physics

PAPER • OPEN ACCESS

Mechanics of tissue competition: interfaces stabilize coexistence

To cite this article: Nirmalendu Ganai *et al* 2019 *New J. Phys.* **21** 063017

View the article online for updates and enhancements.

You may also like

- Dissipative particle dynamics simulations for biological tissues: rheology and competition
Markus Basan, Jacques Prost, Jean-François Joanny et al.
- Interface dynamics of competing tissues
Nils Podewitz, Frank Jülicher, Gerhard Gompper et al.
- A computational study of discrete mechanical tissue models
P Pathmanathan, J Cooper, A Fletcher et al.

This content was downloaded from IP address 103.244.5.250 on 02/10/2026 at 08:35

New Journal of Physics
The open access journal at the forefront of physics

Deutsche Physikalische Gesellschaft DPG
IOP Institute of Physics

Published in partnership with: Deutsche Physikalische Gesellschaft and the Institute of Physics



OPEN ACCESS

RECEIVED
3 March 2019

REVISED
25 April 2019

ACCEPTED FOR PUBLICATION
24 May 2019

PUBLISHED
12 June 2019

Original content from this work may be used under the terms of the Creative Commons Attribution 3.0 licence.

Any further distribution of this work must maintain attribution to the author(s) and the title of the work, journal citation and DOI.



PAPER

Mechanics of tissue competition: interfaces stabilize coexistence

Nirmalendu Ganai[1,2,3], **Tobias Büscher**[1,3], **Gerhard Gompper**[1] and **Jens Elgeti**[1]

[1] Theoretical Soft Matter and Biophysics, Institute of Complex Systems, Forschungszentrum Jülich and JARA, D-52425 Jülich, Germany
[2] Department of Physics, Nabadwip Vidyasagar College, Nabadwip, Nadia 741302, India
[3] These authors contributed equally to this work.

E-mail: j.elgeti@fz-juelich.de

Keywords: tissue competition, tissue growth, homeostatic pressure, particle-based simulations

Abstract

Mechanical forces influence the dynamics of growing tissues. Computer simulations are employed to study the importance of interfacial effects in tissue competition. It was speculated previously that mechanical pressure determines the competition, where the determining quantity is the homeostatic pressure-the pressure where division and apoptosis balance; the tissue with the higher homeostatic pressure overwhelms the other. In contrast, we find that a weaker tissue can persist in stable coexistence with a stronger tissue, if adhesion between them is small enough. An analytic continuum description can quantitatively describe the underlying mechanism and reproduce the resulting pressures and cell-number fractions. Furthermore, simulations reveal a variety of coexisting structures, ranging from spherical inclusions to a bicontinuous state.

1. Introduction

Mechanical forces influence the growth of cells and tissues in several ways, via mechanotransduction [1] or mechanical feedback as regulator of growth and shape [2, 3]. This occurs in systems ranging from plants adapting their growth patterns to mechanical loads [4, 5], all the way to tumors responding in their growth to the pressure of the embedding medium [6–8]. Cells have been shown to differentiate according to substrate stiffness [9], and divide according to mechanical stress and strain [10–16]. Spheroids of many cells, grown in elastic gels [17–19] or shells [20, 21], or even in suspension with osmotic stress [22–25], show strong dependence of growth on the properties of the embedding medium.

Given the evidence of the effect of mechanical stress on growth, it seems clear that mechanics should also influence tissue competition, such as the competition between different mutants in the imaginal wing disk of drosophila [26, 27], or clonal expansion in multistep cancerogenesis [28, 29]. Several theoretical studies support and quantify this idea for both, competition [2] and size determination [30] in the wing, and tumor growth [8, 31].

A tissue grown in a finite compartment exerts a certain pressure onto its surrounding. When reaching a steady state-the homeostatic state-this is the homeostatic pressure P_{H}. Under an external pressure P below P_{H}, the tissue grows; whereas it shrinks if the pressure is above it. This can be formulated as a linear expansion of the bulk growth rate k_{b} around the homeostatic pressure [31],

$$k_{\mathrm{b}} = \kappa(P_{\mathrm{H}} - P) \tag{1}$$

with the pressure response factor κ. To study the role of pressure on growth, cell-culture experiments and computer simulations have been developed to explore this effect [22–24, 32–34]. While confirming the general picture-that mechanical pressure reduces growth-these experiments and simulations have revealed that tissues preferentially divide at the surface, even to the extent that they die (on average) in the bulk and sustain a finite size only by surface growth. While consideration of nutrient transport may be necessary for quantitative description of certain experiments [35, 36], mechanics alone already results in enhanced surface growth, and matches other experiments [33]. For tissue competition in general, and metastatic inefficiency in particular, it has been argued that metastases need to reach a critical size, below which the Laplace pressure from the interfacial tension exceeds the homeostatic pressure difference, and the metastasis disappears [31].

© 2019 The Author(s). Published by IOP Publishing Ltd on behalf of the Institute of Physics and Deutsche Physikalische Gesellschaft

In this work, we study the role of interfacial effects on mechanical tissue competition by numerical simulations, in particular the effect of the strength of adhesive interactions between different tissues. We find that similar to free surfaces, cells divide preferentially at the low-adhesive interfaces. This interfacial growth in turn can stabilize coexistence of two tissues with different homeostatic pressures. Interfaces in tissue competition have been studied mostly from a theoretical perspective. Besides the above mentioned critical size threshold due to interfacial tension, existing studies focus mainly on the propagation of interfaces driven by a difference in homeostatic pressure [34, 37, 38], while the role of an enhanced interfacial growth rate and of interactions across the interface has not yet been considered.

2. Model

Agent-based modelling has been very successful in studying various aspects of tissue growth, such as buckling and stem cell distribution in mammalian skin [39], formation of vascular networks [40] or wound healing [41]. For tumor growth, existing models focus on different stages of tumor progression, e.g. avascular growth [42] , angiogenesis [43] or formation of metastasis [44, 45]. We follow the approach of [32] and model growing and dividing cells by two point-like particles, which repel each other with a growth force

$$\boldsymbol{F}_{ij}^{\mathrm{G}} = \frac{G}{(r_{ij} + r_0)^2}\hat{\boldsymbol{r}}_{ij}, \tag{2}$$

with the growth strength factor G, the distance r_{ij} and unit vector $\hat{\boldsymbol{r}}_{ij}$ between the two particles and a constant r_0. $\boldsymbol{F}_{ij}^{\mathrm{G}}$ is applied during the whole life time of a cell. Cells divide when r_{ij} reaches a certain size threshold r_{ct}. After division, a new particle is placed randomly near each of the particles of the divided cell within a short distance r_{d}. Apoptosis is modeled by a constant rate of cell removal k_{a}. Both processes occur instantaneously. Volume exclusion is maintained by a relatively soft repulsive force $\boldsymbol{F}_{ij}^{\mathrm{V}}$, while adhesion between cells is modeled by a constant attractive force $\boldsymbol{F}_{ij}^{\mathrm{A}}$, given by

$$\boldsymbol{F}_{ij}^{\mathrm{V}} = f_0\left(\frac{R_{\mathrm{PP}}^5}{r_{ij}^5} - 1\right)\hat{\boldsymbol{r}}_{ij}, \tag{3}$$

$$\boldsymbol{F}_{ij}^{\mathrm{A}} = -f_1\hat{\boldsymbol{r}}_{ij}, \tag{4}$$

with the strength of volume exclusion and adhesion force f_0 and f_1, respectively. R_{PP} is the cut-off length of pairwise particle interactions. Division threshold r_{ct}, the constant r_0 in equation (2) as well as R_{PP} are all of the order of the typical cell size. A dissipative particle dynamics (DPD)-type thermostat is employed to account for dissipation of energy and random fluctuations, which mimics the stochasticity of many biological processes, e.g. the dynamic structure of the cytoskeleton or interactions with the extracellular matrix. The thermostat consists of a dissipative force

$$\boldsymbol{F}_{ij}^{\mathrm{D}} = -\gamma\omega^{\mathrm{D}}(r_{ij})(\hat{\boldsymbol{r}}_{ij}\cdot\boldsymbol{v}_{ij})\hat{\boldsymbol{r}}_{ij}, \tag{5}$$

with the strength γ, a weight function $\omega^{\mathrm{D}}(r_{ij})$ and the relative velocity $\boldsymbol{v}_{ij} = \boldsymbol{v}_j - \boldsymbol{v}_i$, as well as a random force

$$\boldsymbol{F}_{ij}^{\mathrm{R}} = \sigma\omega^{\mathrm{R}}(r_{ij})\xi_{ij}\hat{\boldsymbol{r}}_{ij}, \tag{6}$$

with strength $\sigma = \sqrt{2k_{\mathrm{B}}T\gamma}$, a Gaussian random variable ξ_{ij} with zero mean and unit variance and a weight function $\omega^{\mathrm{R}}(r_{ij}) = \sqrt{\omega^{\mathrm{D}}(r_{ij})}$. T is an effective temperature which characterizes the strength of the fluctuations. Its value is chosen such that cells do not get stuck in local minima but has no noticeable effect otherwise.

The dynamics of particle i is then determined by

$$m_i\ddot{\boldsymbol{r}}_i = \boldsymbol{F}_{ik}^{\mathrm{G}} + \boldsymbol{F}_{ik}^{\mathrm{D}} + \boldsymbol{F}_{ik}^{\mathrm{R}} + \sum_{j\neq i,k}(\boldsymbol{F}_{ij}^{\mathrm{A}} + \boldsymbol{F}_{ij}^{\mathrm{V}} + \boldsymbol{F}_{ij}^{\mathrm{D}} + \boldsymbol{F}_{ij}^{\mathrm{R}}) + \boldsymbol{F}_i^{\mathrm{B}}, \tag{7}$$

with mass m_i of particle i, particle k that forms a cell with particle i, and the background dissipation force $\boldsymbol{F}_i^{\mathrm{B}} = -\gamma_{\mathrm{b}}\mathbf{v}_i$. We integrate the equations of motion with a self-consistent velocity-Verlet algorithm. Note that the division rate k_{d} is not fixed, but is obtained from the simulations and depends on the other model parameters.

This model results in pressure-dependent growth, in reasonable agreement with experiments [22–24, 32–34]. For two competing tissues A and B, parameters for each tissue can be set independently. In this work, we only vary the growth strengths G^{A} and G^{B}, the self adhesion strengths f_1^{AA}, f_1^{BB} and the cross-adhesion strength $f_1^{\mathrm{AB}} \coloneqq f_{\mathrm{c}}$. We define a reference tissue (see SI for numerical values) and report parameters in terms of this reference tissue, denoted by a dagger, e.g. $G^{\dagger} = G/G_0$. We measure space in units of the pair potential interaction range R_{PP}, time by the inverse of the apoptosis rate k_{a}, force in units of G_0/R_{PP}^2 and thus stress by G_0/R_{PP}^4. Quantities measured in these units are denoted by an asterisk *.

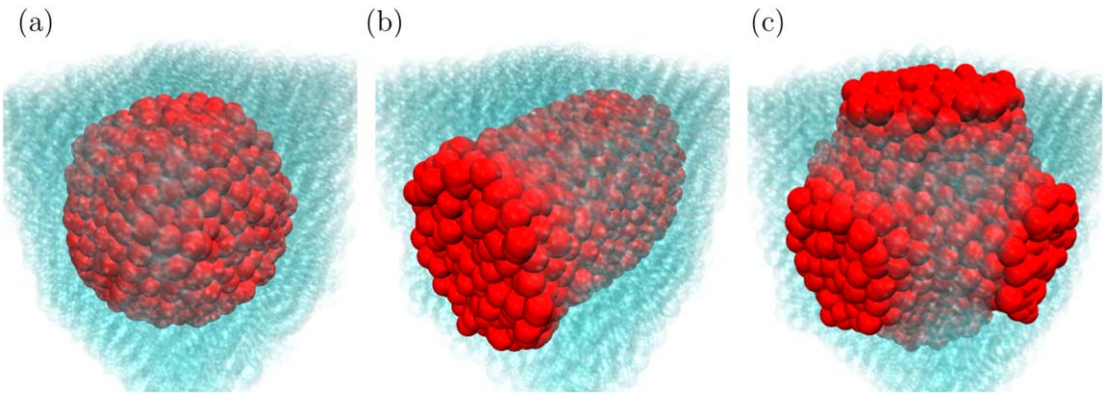

Figure 1. Snapshots of various structures of tissue coexistence. Both tissues are identical (reference tissue), interacting via $f_c = 0$. (a) Spherical inclusion. (b) Cylindrical inclusion. (c) Schwarz-P like bicontinuous structure. Other structures observed include flat interfaces, perforated lamellar, combinations (e.g. perforated lamellar together with a spheroid), and inverted (e.g. inverse spheroid) structures.

3. Results

Very small *cross-adhesion* strengths f_c between cells of different tissues (i.e. $f_c \ll \min(f_1^{AA}, f_1^{BB})$) result in fundamentally different outcomes of the tissue competition than predicted from simply assuming increased surface tension [31]. Instead of one tissue overwhelming the other for different homeostatic pressures or the existence of a critical size threshold explained above, we observe stable coexistence in a variety of segregated structures depending on initial conditions (see figure 1). While segregation of the tissues can be expected because of the high interfacial tension ($\gamma^{AB} \gg \gamma^{AA}, \gamma^{BB}$) [46], the stable coexistence comes at a surprise. Even for two identical tissues (i.e the same tissue parameters but dissimilar cells, with cross-adhesion different from self-adhesion) a single A cell in a host of B grows into a stable spheroid occupying about a third of the volume. Similarly, a random 1:2 mixture of stronger A cells in a host of B can result in a stable 3:1 Schwarz-P bicontinuous structure. Movie 1 and 2 in the SI show the temporal evolution during simulations similar to these two scenarios.

3.1. Flat interfaces-origin of coexistence

In order to understand the underlying physical mechanism of this behaviour, we turn to a simpler geometry of a slab-like tissue arrangement and develop an appropriate analytic model. Cells are confined to a finite (periodic) compartment of size $L_x \times L_y \times L_z$. All cells in the left half ($z < L_z/2$) are type B cells, all others type A. Due to the periodic boundary conditions, the system contains two interfaces. Large adhesion between cells of the same tissue and no adhesion between cells of different tissues leads to a large interfacial tension, stabilizing the flat interface with nearly vanishing roughness. This allows the measurement of the division rate k_d as a function of the distance to the interface. The growth rate profile (see figure 2(b)) reveals that cells divide more in a small region of width a (roughly the cut-off length R_{PP}, with a weak dependence on other model parameters) at the interface. In the bulk of the tissue, the net growth rate is negative due to an elevated pressure. These results motivate a two-rate growth model [22–24, 32, 33]

$$\partial_t \rho(s) + \nabla \cdot (\rho(s)\boldsymbol{v}) = k_b \rho(s) + \Delta k_s \Theta(s - a)\rho(s), \tag{8}$$

where $\rho(s)$ is the cellular density of either tissue, Θ the Heaviside step function, s the distance to the nearest interface and $\boldsymbol{v}$ the cell-velocity field. The additional growth at the interface is modeled as a growth rate enhancement Δk_s near the interface (less than a away).

Division and apoptosis events locally relax stress and thus lead to a liquefaction of the tissue on long timescales [47–49]. Indeed, some experiments on tissue rheology suggest liquid behaviour on long timescales [50–52], while some other experiments on drosophila wing discs suggest that not all stress is relaxed by growth [53–55]. However, our model tissue clearly behaves as a liquid [47]. With the low velocities (cells move a few cell diameters at most during their lifetime) and no external forcing, we can thus assume a constant pressure across the system. Within a sharp-kink approximation with constant density $\rho(s) = \rho_0$ we integrate equation (8) over space, which gives for the total cell number N_A of tissue A

$$\partial_t N_A = k_b^A N_A + \Delta k_s^A \rho_0 2a L_x L_y, \tag{9}$$

and similarly for tissue B. We define the cell number fraction $\phi = L_A/L_z = N_A/(N_A+N_B)$ of type A cells, and divide equation (9) by $(N_A+N_B) = \rho_0 L_x L_y L_z$ and obtain

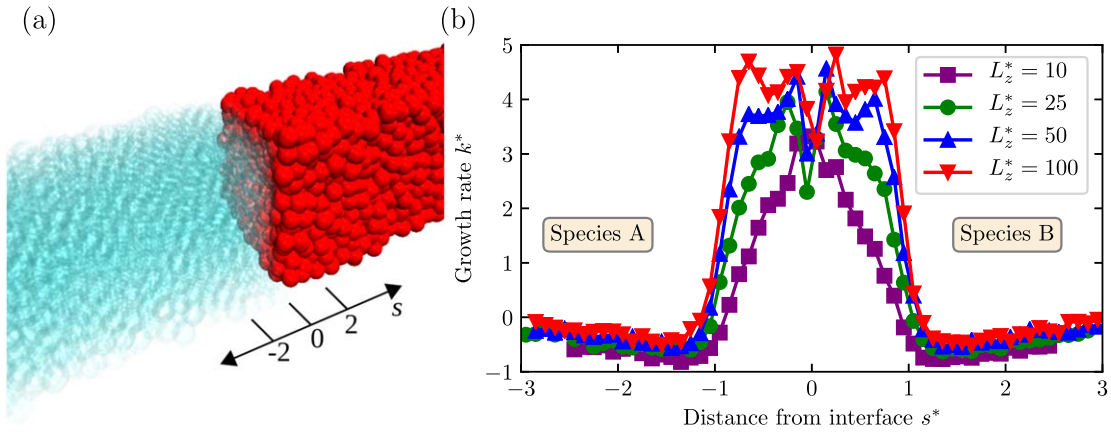

Figure 2. Planar interface between two competing tissues. (a) Simulation snapshot. (b) Net growth rate $k^* = (k_d - k_a)/k_a$ as a function of the distance from the interface s^* for the competition between two identical (reference) tissues with $f_c = 0$ for various box lengths L_z^*.

$$\partial_t \phi = k_b^A \phi + 2a\Delta k_s^A / L_z, \tag{10}$$

for tissue A, and

$$\partial_t (1 - \phi) = k_b^B (1 - \phi) + 2a\Delta k_s^B / L_z, \tag{11}$$

for tissue B. The homogeneous pressure motivates the linear dependence of k_b on $(P_H - P)$ as in equation (1), and similarly $\Delta k_s \simeq \Delta k_s^0 + \Delta k_s^1 (P_H - P)$.

For simplicity, we first explore two identical tissues. Insertion of the linear pressure dependence of k_b and Δk_s in equation (10) and (11) yields the pressure

$$P = P_H + \frac{4a\Delta k_s^0}{(4a\Delta k_s^1 + \kappa L_z)}, \tag{12}$$

i.e. the additional growth at the interface elevates the pressure above the homeostatic pressure, which in turn causes the negative net growth rate in the bulk. Similarly, from equations (10) and (11), we obtain

$$\phi(t) = \frac{1}{2} + \left(\phi_0 - \frac{1}{2}\right) e^{-\kappa (P - P_H) t}, \tag{13}$$

with the initial number fraction ϕ_0. Thus, the number fractions of two tissues with identical parameters, but no cross-adhesion, will relax exponentially towards 1/2.

We determine the bulk parameters P_H, κ from bulk simulations as in [33] by using the virial stress

$$\sigma_{\alpha\beta} = -\frac{1}{V}\left[\sum_i m_i v_\alpha^i v_\beta^i + \sum_{i,j} r_\alpha^{ij} f_\beta^{ij}\right]. \tag{14}$$

Here, $\sum_i$ sums over all particles, v_α^i is the α component of the velocity of particle i, $\sum_{i,j}$ sums over all interacting pairs of particles, r_α^{ij} is the α component of the distance vector between i and j and f_β^{ij} the β component of the force on particle i due to j. The mean pressure is $P = -1/3\,\mathrm{Tr}\langle\sigma_{\alpha\beta}\rangle$. The pressue response coefficient κ is obtained as the slope of a linear fit to the growth rates k for different pressures P around the homeostatic pressure P_H. We use a constant-pressure ensemble to impose a pressure P_i [33], where the pressure is imposed by periodic rescaling of the volume of the simulation box by a factor

$$\chi = 1 - \beta_T \frac{\Delta t}{t_P}(P - P_i), \tag{15}$$

with isothermal compressibility β_T, simulation time step Δt and relaxation time t_P. In order to measure the interface growth coefficients $a\Delta k_s^0$, $a\Delta k_s^1$ we make use of mirror boundary conditions. Particles closer to the boundary than $R_{PP}/2$ interact with the mirrored image of themselves as they would with a particle of the other tissue. We employ the mirror boundary conditions in z-direction and measure the average pressure for different box lengths L_z. $a\Delta k_s^0$, $a\Delta k_s^1$ are obtained by fitting equation (12) to simulation results. As shown in [33], the homeostatic pressure grows approximately linearly with G, and decreases linearly with f_1. κ is essentially independent of f_1, but decreases linearly with G. The interface growth coefficient $a\Delta k_s^0$ is only weakly dependent on G, but grows linearly with f_1, while $a\Delta k_s^1$ does not show a clear dependence on tissue parameters (see figures in SI). With the parameters determined independently, equations (12) and (13) reproduce the simulations without further parameter adjustment (see figure 3).

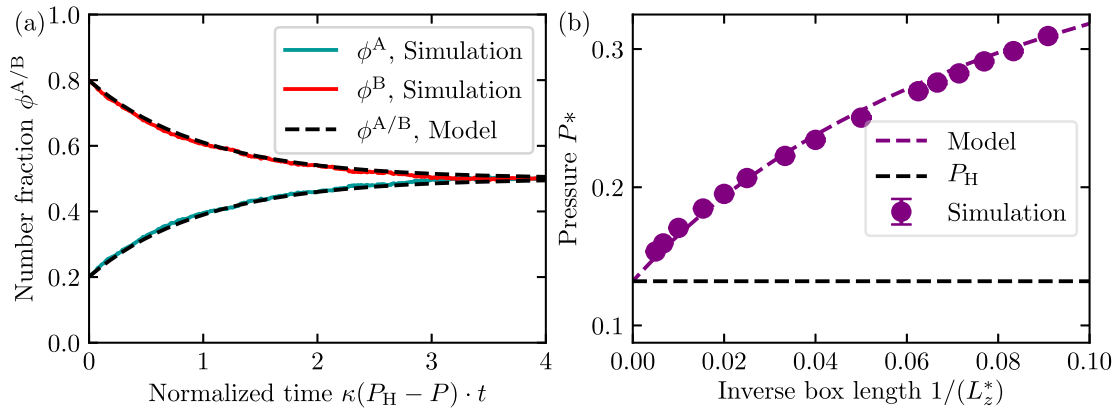

Figure 3. (a) Solid cyan and red lines show the time evolution of the cell number fractions $\phi^{A/B}$ in a competition with zero cross-adhesion $f_c = 0$ between two identical (reference) tissues for a box length $L_z^* = 100$. Dashed black lines show equation (13) for both tissues with parameters fixed by independent simulations. (b) Average pressure measured in competition as in (a) in terms of the inverse box length L_z^*. Dashed purple line shows equation (12), with parameters as in (a). Errors are determined by block averaging method (see. [56]).

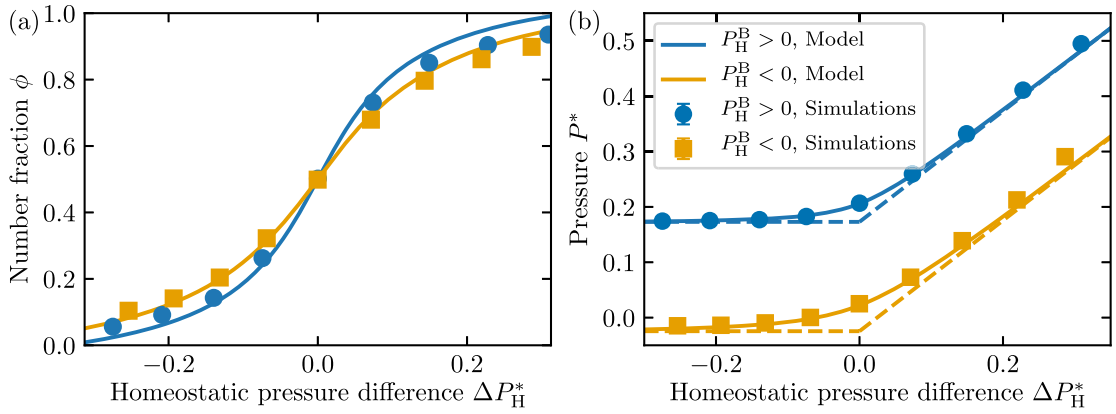

Figure 4. (a) Cell number fractions ϕ for various homeostatic pressure differences ΔP_H^*. Tissue B is fixed (as reference tissue (blue bullets) and as one with a higher growth force strength and a higher cell–cell adhesion coefficient (yellow squares)) and the homeostatic pressure of tissue A is varied. Symbols are simulation results while the solid lines are predictions by the two-rate model according to equation (17), using the parameters of tissue B. See table S2 in the SI for numerical values of the simulation and model parameters of the two fixed tissues. (b) Average pressure measured during the simulations shown in (a) together with a plot of equation (16), using the parameter of tissue B. The results are not symmetric around $\Delta P_H = 0$ because tissue B is fixed. Dashed lines are lower bounds from $L^{A,B} < L_z$. Boxsize $L_x^* = L_y^* = 7$; $L_z^* = 40$. Errors are determined by block averaging method.

3.2. Competition with flat interface

Next, we explore the competition between two tissues with different homeostatic pressures with a planar interface. We balance the pressures on both sides of the interface and obtain

$$P = P_H^A + \frac{2a\Delta k_s^{0A}}{(2a\Delta k_s^{1A} + \kappa^A L^A)} = P_H^B + \frac{2a\Delta k_s^{0B}}{(2a\Delta k_s^{1B} + \kappa^B L^B)}, \tag{16}$$

where L^B and $L^A (= L_z - L^B)$ are the lengths occupied by tissue A and B. Note that the insertion of $L^{A,B} < L_z$ in equation (16) gives a lower bound for the pressure: the system pressure is always larger than the homeostatic pressure of the stronger tissue, plus a system-size-dependent constant. Indeed, this lower bound describes the pressure rather well. The stronger tissue occupies the larger part of the system, and thus $L^{\text{'stronger'}} \approx L_z$. Thus, for fixed host tissue B, the pressure is almost constant for $\Delta P_H \equiv P_H^B - P_H^A < 0$, and grows almost linearly for $\Delta P_H > 0$ (see figure 4(b)). The weaker tissue supports the higher pressure by decreasing in size, and thus its apoptotic volume, sustained by interface growth. In simulations, tissue B is fixed and the growth force strength G of tissue A is varied in order to change its homeostatic pressure. Simulations for two different fixed tissues are performed, the reference tissue and one with a higher growth force strength and a higher cell–cell adhesion coefficient, which results in a negative homeostatic pressure. For the simulated tissues, the parameter κ, Δk_s^0 and Δk_s^1 only show small variations with G (see SI). We therefore assume them to be the same for both tissues to obtain

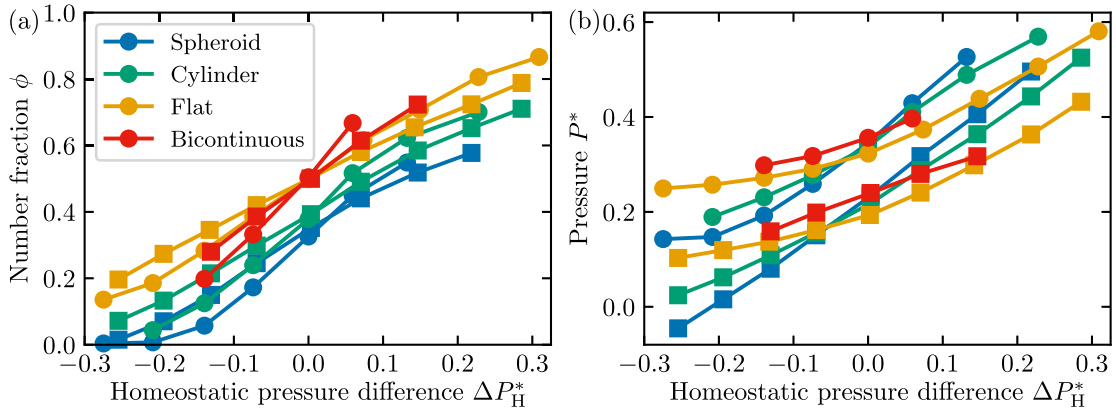

Figure 5. Cell number fractions ϕ for different homeostatic pressure differences ΔP_H^* and different structures, as indicated by color. Circles correspond to a positive homeostatic pressure of tissues B and squares to a negative one (same parameters as in figure 4, except cubic box size $L^* = 10$). (b) Average pressure measured in the simulations shown in (a). $L_x^* = L_y^* = L_z^* = 10$. Errors are determined by block averaging method.

$$\phi = \frac{1}{2} + \frac{2a\Delta k_s^0}{\kappa \Delta P_H L_z} \pm \left[\left(\frac{2a\Delta k_s^0}{\kappa \Delta P_H L_z}\right)^2 + \left(\frac{1}{2} + \frac{2a\Delta k_s^1}{\kappa L_z}\right)^2\right]^{\frac{1}{2}}. \tag{17}$$

Note that for $\Delta P_H \to 0$, equation (17) reproduces $\phi = 1/2$ as expected. Around $\Delta P_H = 0$, ϕ grows linearly with ΔP_H and then slows down (see figure 4(a)). For large differences in homeostatic pressure, the model predicts two interfaces less than $2a$ apart, thus violating its assumptions, and consequently fails to predict the simulation results properly. Equations (16) and (17) reproduce simulation results well (see figure 4) in a broad parameter range. Note that this also holds true for negative homeostatic bulk pressures.

3.3. Non-planar interfaces

These results show that indeed the enhanced growth at the interface lies at the heart of tissue coexistence observed in our simulations. However, a flat interface is not the only stable structure for two competing tissues. Depending on initial conditions and parameters, a large range of other structures can be found (see figure 1). These different structures result in different interface-to-volume ratios (and possibly other interfacial effects, e.g. due to curvature of the interface), changing the steady-state volume fractions and pressures. We present simulation results for these structures in figure 5. Simulations are started from initial conditions morphologically similar to the final structure, but with an initial number fraction different than that at steady state.

Compared to flat interfaces, the number fraction ϕ of tissues in spherical or cylindrical configuration is smaller, with spheroids being smaller than cylinders. Spheroids become unstable with growing homeostatic pressure difference (around $\Delta P_H^* \approx 0.2$). They then transform into cylinders, which again become unstable with further increasing homeostatic pressure difference around $\Delta P_H^* \approx 0.3$ and turn into a slab-like structure, which becomes unstable as well at even larger ΔP_H^* and turns into inverted structures. Vice versa, cylinders turn into spheroids if the difference in homeostatic pressure is very negative ($\Delta P_H^* \approx -0.3$). The number fraction of the bicontinuous phase is roughly the same as for flat interfaces, but the bicontinuous phase is only stable in a small regime ($\Delta P_H^* \approx [-0.15,\ 0.15]$ for $P_H^B < 0$). For larger ΔP_H, the bicontinuous structure turns into a perforated lamellar phase of the weaker tissue inside the stronger tissue. The stability limits of the individual phases can be estimated in figure 5, where data is only shown within the respective stability regime. In general, the number fraction ϕ of all structures changes sigmoidally with homeostatic pressure difference.

While all of these structures are very stable over time, the question arises how stable they are when the interfacial effects become smaller. We study this effect numerically, by observing the structures for two identical tissues formed under zero cross-adhesion and continuously increase the cross-adhesion strength f_c to the value of self-adhesion strength (i.e. $f_c = f_1^{AA} = f_1^{BB}$). Figure 6 shows that all structures remain almost unchanged up to a cross-adhesion f_c approximately two thirds of the self adhesion f_1. For higher f_c, only a mixed, sponge-like state remains. Mixing occurs before cross-adhesion strength reaches self-adhesion strength because of the active growth. The total adhesion force $\boldsymbol{F}_i^{A,tot} = \sum_j \boldsymbol{F}_{ij}^A$ on a particle i close to the interface acts perpendicular to the interface towards the tissue species of i. The amplitude of this force decreases linearly towards zero when cross-adhesion strength approaches self-adhesion strength, thus, at some value $f_c < f_1$ the active growth force $\boldsymbol{F}_i^G$ overcomes the total adhesive force and the interface becomes unstable.

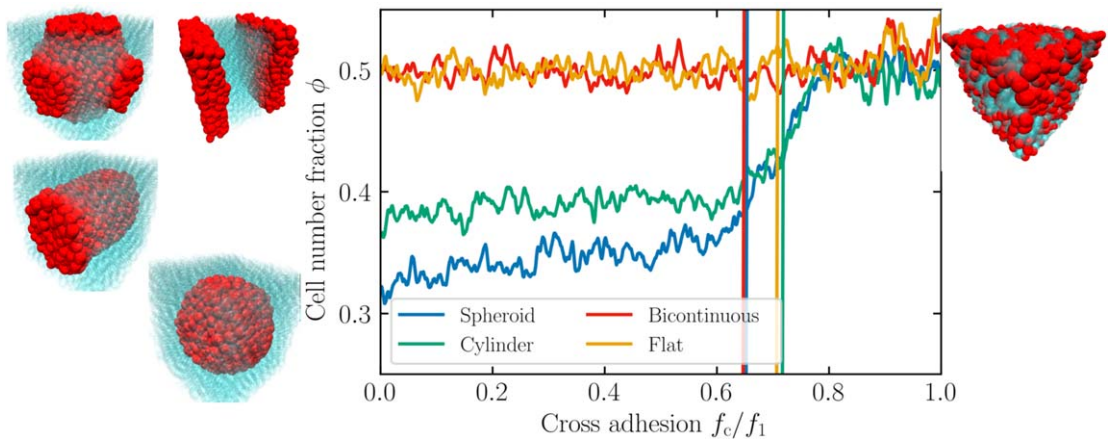

Figure 6. Variation of cell number fraction ϕ with time with increasing cross-adhesion $f_c/f_1 = t^*/240$ between two identical (reference) tissues. Simulations are started from spherical (blue) and cylindrical inclusions (green) of tissue A in B as well as from flat interfaces (yellow) and a bicontinuous phase (red). Solid vertical lines are marking transition points after which cells start to detach from the initial structures. Cubic box size $L^* = 10$. Simulation snapshots at the sides show initial and final configurations.

4. Conclusions

In summary, the interface between two tissues plays an important role in the competition between them. The enhanced growth at the interface can stabilize coexisting phases even when one tissue has a higher homeostatic pressure. The coexisting phase appears in a variety of different structures, ranging from a spherical inclusion over a flat interface to a bicontinuous structure.

Interesting future directions are interfacial dynamics, roughness, and shapes, as previously explored for tissues on substrates and without additional interfacial growth [34, 37, 38]. Vice versa, it would be interesting to add interfacial growth to tissues growing on substrates.

Finally, our results tentatively suggest an explanation for tumor heterogeneity and the abundance of occult tumors: small symptom-free micro-tumors that are frequently found in the human body [57]. For the thyroid, it might even be 'normal' to find microscopic lesions [58]. Our results provide a possible mechanical explanation how coexistence of different tissues can be stabilized. For example, a mutation might downregulate cadherins-an important cellular adhesion protein-as it often happens in tumors [59]. While this might reduce survival signaling [60], the lack of adhesion could favour our mechanism of coexistence, even for weaker tissue growth.

Acknowledgments

The authors gratefully acknowledge the computing time granted through JARA-HPC on the supercomputer JURECA [61] at Forschungszentrum Jülich

ORCID iDs

Tobias Büscher https://orcid.org/0000-0002-5009-1479
Gerhard Gompper https://orcid.org/0000-0002-8904-0986
Jens Elgeti https://orcid.org/0000-0001-7300-0923

References

[1] Wozniak M A and Chen C S 2009 *Nat. Rev. Mol. Cell Biol.* **10** 34–43
[2] Shraiman B I 2005 *Proc. Natl Acad. Sci. U. S. A.* **102** 3318–23
[3] Irvine K D and Shraiman B I 2017 *Development* **144** 4238
[4] Jarvis M, Briggs S and Knox J 2003 *Plant Cell Environ.* **26** 977–89
[5] Coen E, Kennaway R and Whitewoods C 2017 *Development* **144** 4203–13
[6] Kumar S and Weaver V M 2009 *Cancer Metastasis Rev.* **28** 113–27
[7] Butcher D T, Alliston T and Weaver V M 2009 *Nat. Rev. Cancer* **9** 108–22
[8] Taloni A, Ben Amar M, Zapperi S and La Porta C A 2015 *Eur. Phys. J. Plus* **130** 224
[9] Engler A J, Sen S, Sweeney H L and Discher D E 2006 *Cell* **126** 677–89
[10] Nelson C M, Jean R P, Tan J L, Liu W F, Sniadecki N J, Spector A A and Chen C S 2005 *Proc. Natl Acad. Sci. U.S.A.* **102** 11594–9
[11] Cheng G, Tse J, Jain R K and Munn L L 2009 *PLoS One* **4** 1–11

[12] Fink J et al 2011 Nat. Cell Biol. 13 771
[13] Uyttewaal M et al 2012 Cell 149 439–51
[14] Streichan S J, Hoerner C R, Schneidt T, Holzer D and Hufnagel L 2014 Proc. Natl Acad. Sci. U.S.A. 111 5586–91
[15] LeGoff L and Lecuit T 2015 Cold Spring Harbor Perspect. Biol. 8 a019232
[16] Eder D, Aegerter C and Basler K 2017 Mech. Dev. 144 53–61
[17] Helmlinger G, Netti P A, Lichtenbeld H C, Melder R J and Jain R K 1997 Nat. Biotechnol. 15 778–83
[18] Gordon V D, Valentine M T, Gardel M L, Andor-Ardo D, Dennison S, Bogdanov A A, Weitz D A and Deisboeck T S 2003 Exp. Cell Res. 289 58–66
[19] Kaufman L J, Brangwynne C P, Kasza K E, Filippidi E, Gordon V D, Deisboeck T S and Weitz D A 2005 Biophys. J. 89 635–50
[20] Alessandri K et al 2013 Proc. Natl Acad. Sci. U.S.A. 110 14843–8
[21] Domejean H, Saint Pierre M D L M, Funfak A, Atrux-Tallau N, Alessandri K, Nassoy P, Bibette J and Bremond N 2017 Lab. Chip 17 110–9
[22] Montel F et al 2011 Phys. Rev. Lett. 107 188102
[23] Montel F, Delarue M, Elgeti J, Vignjevic D, Cappello G and Prost J 2012 New J. Phys. 14 055008
[24] Delarue M, Montel F, Caen O, Elgeti J, Siaugue J M, Vignjevic D, Prost J, Joanny J F and Cappello G 2013 Phys. Rev. Lett. 110 138103
[25] Taloni A, Alemi A A, Ciusani E, Sethna J P, Zapperi S and La Porta C A M 2014 PLoS One 9 e94229
[26] Morata G and Ripoll P 1975 Dev. Biol. 42 211–21
[27] Diaz B and Moreno E 2005 Exp. Cell. Res. 306 317–22
[28] Moolgavkar S H and Luebeck E G 2003 Genes. Chromosomes Cancer 38 302–6
[29] Meza R and Chang J T 2015 BMC Public Health 15 789
[30] Hufnagel L, Teleman A A, Rouault H, Cohen S M and Shraiman B I 2007 Proc. Natl Acad. Sci. U. S. A. 104 3835–40
[31] Basan M, Risler T, Joanny J F, Sastre-Garau X and Prost J 2009 HFSP J 3 265–72
[32] Basan M, Prost J, Joanny J F and Elgeti J 2011 Phys. Biol. 8 026014
[33] Podewitz N, Delarue M and Elgeti J 2015 Europhys. Lett. 109 58005
[34] Podewitz N, Jülicher F, Gompper G and Elgeti J 2016 New J. Phys. 18 083020
[35] Jagiella N, Mueller B, Mueller M, Vignon-Clementel I E and Drasdo D 2016 PLoS Comput. Biol. 12 1–39
[36] Hornung R, Grünberger A, Westerwalbesloh C, Kohlheyer D, Gompper G and Elgeti J 2018 J. R. Soc. Interface 15 20170713
[37] Ranft J, Aliee M, Prost J, Jülicher F and Joanny J F 2014 New J. Phys. 16 035002
[38] Williamson J J and Salbreux G 2018 Phys. Rev. Lett. 121 238102
[39] Kobayashi Y, Yasugahira Y, Kitahata H, Watanabe M, Natsuga K and Nagayama M 2018 Npj Comput. Mater. 4 45
[40] van Oers R F M, Rens E G, LaValley D J, Reinhart-King C A and Merks R M H 2014 PLoS Comput. Biol. 10 1–14
[41] Walker D C, Hill G, Wood S M, Smallwood R H and Southgate J 2004 IEEE Trans. Nanobiosci. 3 153–63
[42] Drasdo D and Hoehme S 2005 Phys. Biol. 2 133–47
[43] Welter M, Bartha K and Rieger H 2009 J. Theor. Biol. 259 405–22
[44] Wynn M M, Kulesa P and Schnell S 2012 J. R. Soc. Interface 9 1576–88
[45] Norton K A and Popel A S 2014 J. R. Soc. Interface 11 20140640
[46] Foty R and Steinberg M 2004 Int. J. Dev. Biol. 48 397–409 S
[47] Ranft J, Basan M, Elgeti J, Joanny J F, Prost J and Jülicher F 2010 Proc. Natl Acad. Sci. U. S. A. 107 20863–8
[48] Khalilgharibi N, Fouchard J, Recho P, Charras G and Kabla A 2016 Curr. Opin. Cell Biol. 42 113–20
[49] Matoz-Fernandez D A, Agoritsas E, Barrat J L, Bertin E and Martens K 2017 Phys. Rev. Lett. 118 158105
[50] Phillips H M and Steinberg M S 1978 J. Cell Sci. 30 1–20
[51] Guevorkian K, Colbert M J, Durth M, Dufour S and Brochard-Wyart F 2010 Phys. Rev. Lett. 104 218101
[52] Gonzalez-Rodriguez D, Bonnemay L, Elgeti J, Dufour S, Cuvelier D and Brochard-Wyart F 2013 Soft Matter 9 2282–90
[53] LeGoff L, Rouault H and Lecuit T 2013 Development 140 4051–9
[54] Mao Y, Tournier A L, Hoppe A, Kester L, Thompson B J and Tapon N 2013 EMBO J. 32 2790–803
[55] Pan Y, Heemskerk I, Ibar C, Shraiman B I and Irvine K D 2016 Proc. Natl Acad. Sci. U.S.A. 113 E6974–83
[56] Allen M P and Tildesley D J 1989 Computer Simulation of Liquids (Oxford: Clarendon Press)
[57] Bissell M J and Hines W C 2011 Nat. Med. 17 320–9
[58] Harach H R, Franssila K O and Wasenius V M 1985 Cancer 56 531–8
[59] Weinberg R A 2007 The Biology of Cancer (New York: Garland Science)
[60] Alberts B, Johnson A, Lewis J, Raff M, Roberts K and Walter P 1994 Molecular Biology of the Cell 3rd edn (New York: Garland Science)
[61] Jülich Supercomputing Centre 2018 J. Large-Scale Res. Facil. 4 A132